JOURNAL OF SPACECRAFT AND ROCKETS
Vol. 33, No. 1, January–February 1996

Atmospheric Research with the Small Expendable Deployer System: Preliminary Analysis

Michele Grassi*
University of Naples "Federico II," Naples 80125, Italy
and
Mario L. Cosmo†
Smithsonian Astrophysical Observatory, Cambridge, Massachusetts 02138

Data on the structure of the lower thermosphere are extremely limited because of the inaccessibility of this region to research vehicles. Downward-deployed tethered satellites can provide access to this region of the atmosphere. A preliminary analysis of the potential use of the end mass of the Small Expendable Deployer System as a scientific platform for atmospheric and aerothermodynamic research is presented. To this end, the deployment and attitude dynamics of the end mass during the first mission have been numerically simulated. It is shown that measurements of the atmospheric mean density with the end-mass onboard accelerometers can be performed only in a short time interval around the orbit perigee; in addition, the analysis of the payload attitude dynamics shows the need for attitude control. A preliminary analysis of end-mass attitude control techniques is then performed. Results show that the stringent attitude control requirements can be satisfied by active control devices.

Nomenclature

A_F	= fin surface
A_i	= cross section of the ith lumped mass
A_p	= payload cross section
$\boldsymbol{a}_{\text{c.m.}}$	= acceleration vector of the payload center of mass
$a_D, \boldsymbol{a}_D$	= acceleration due to the aerodynamic drag (modulus, vector)
$\boldsymbol{a}_T$	= vector of the payload acceleration due to the tether tension
B	= rigid boom length
c_D	= drag coefficient
$\boldsymbol{D}_i$	= aerodynamic drag vector acting on the ith lumped mass
$\boldsymbol{D}_p$	= aerodynamic drag vector acting on the payload
d	= fin arm length
I_1, I_2, I_3	= principal moments of inertia of the payload
k_α, k_β	= gains of the roll and pitch control laws
l_1	= length of the tether segment adjacent to the payload
M_{ci}	= ith body component of the attitude-control torque
M_{ei}	= ith body component of the external torques
M_i	= ith body component of the total torque
m_p	= payload mass
$\hat{\boldsymbol{N}}_i$	= unit vector of the direction perpendicular to the surface A_i
$T, \boldsymbol{T}$	= tether tension measured at the payload (modulus, vector)
$V_{\text{c.m.}}$	= modulus of payload center-of-mass velocity relative to the atmosphere
$V_i, \hat{\boldsymbol{V}}_i$	= velocity relative to the atmosphere of the ith lumped mass (modulus, unit vector)
X, Y, Z	= inertial reference frame
x, y, z	= orbiting reference frame with origin at the payload center of mass
x_0, y_0, z_0	= orbiting reference frame with origin at the initial position of the system center of mass
x_1, x_2, x_3	= body coordinates of the tether attachment point
α, β, γ	= roll, pitch, and yaw angles of the payload
δ	= payload ejection angle with respect to the local vertical
$\varepsilon_1, \varepsilon_2$	= in-plane and out-of-plane tether lateral deflections
ζ	= damping factor
η	= angle between the normal to the fin surface and the 1 axis of the body reference frame
ρ	= atmospheric density
τ_α, τ_β	= roll and pitch time constants
Ω	= orbital angular velocity
ω_i	= ith body component of the payload inertial angular velocity
1, 2, 3	= payload principal reference frame

Subscripts

max	= maximum value
ss	= steady-state value

Received Aug. 3, 1994; revision received June 9, 1995; accepted for publication June 12, 1995.

*Researcher, Dipartimento di Scienza e Ingegneria dello Spazio, P. Le Tecchio 80. Member AIAA.
†Staff Scientist, 60 Garden Street. Member AIAA.

Introduction

ATMOSPHERIC science data in the region between 90 and 250 km have been collected only by sounding rockets and satellites in highly elliptic orbits under transitory conditions, or by the reentering Space Shuttle.[1,2] Therefore, satellites flying at constant altitude in the lower thermosphere can give access in a global sense to this region of the atmosphere.

Downward-deployed tethered satellites can provide the tool for in situ exploration of the Earth's upper atmosphere. NASA has evaluated the feasibility of Shuttle-based flights to deploy instrumented platforms in the lower thermosphere.[3] Recently a series of low-cost tether missions has been performed by using the Small Expendable Deployer System (SEDS). SEDS first flights[4,5] deployed a 25-kg instrumented payload with a 20-km-long tether from a Delta second stage at the apogee (730 km) of an orbit with an inclination of 34 deg and a perigee of 184 km.

Since several flights with different orbit characteristics are required to provide for local time, seasonal, and latitude variation effects on the Earth's atmosphere, SEDS first flights have been mainly intended to collect data on the tether and payload attitude dynamics by means of the onboard instrumentation (a three-axis accelerometer, a three-axis load cell, and magnetometers).[6] Nevertheless, SEDS can represent a precursor for future tethered satellites for atmospheric research.[7]

Various authors have analyzed the dynamics of SEDS. The deployment maneuver has been investigated considering different

Table 1 Payload mass, principal moments of inertia, initial angular rates, and tether attachment-point coordinates

Payload mass, kg	Principal moments of inertia, kg m^2			Initial angular rates, deg/s			Attachment-point coordinates, m		
	I_1	I_2	I_3	ω_1	ω_2	ω_3	x_1	x_2	x_3
25	0.290	0.468	0.550	5.13	0	5.92	−0.187	−0.035	−0.162

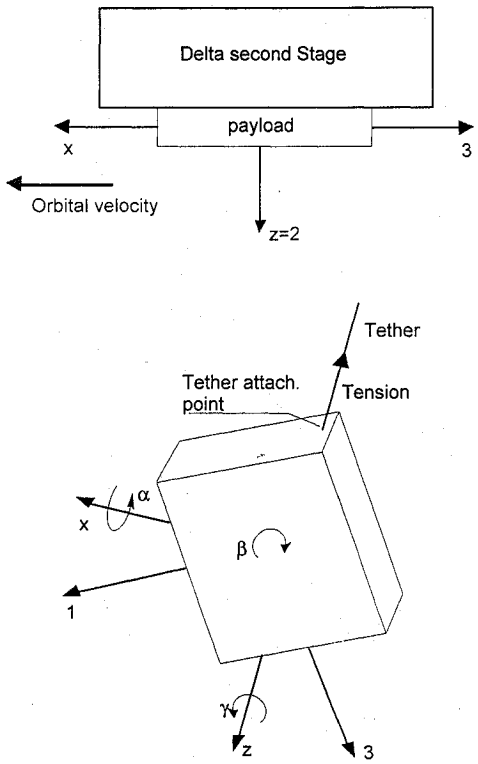

Fig. 1 Payload attitude angles and reference frames.

options and tether tension control laws. The parameters characterizing the SEDS deployment phase, such as tether deployment velocity, tension, and length, have been widely investigated to identify the optimum deployment maneuver.[4–6]

This paper presents a preliminary analysis of SEDS's payload as an instrumented platform for atmospheric and aerothermodynamic research. To this end, numerical simulations of the first SEDS mission (SEDS-1) are performed to evaluate the acceleration levels onboard the payload, and to investigate the possibility of measuring the atmospheric density from the accelerometer simulated data. The need for attitude control is stressed by the analysis of the payload attitude dynamics. A preliminary analysis of end-mass attitude control techniques is finally presented by using simplified analytical models and numerical simulations.

System Configuration

With reference to Fig. 1, the payload is schematized as a rigid parallelepiped. The payload angular orientation is described with the three Euler angles (roll, pitch, and yaw) relative to a right-handed reference frame co-orbiting with the payload. The origin of this frame is located at the payload center of mass, the z axis coincides with the payload position vector and is directed toward the Earth, the y axis is perpendicular to the orbital plane, and the x axis completes the right-handed reference frame (see Fig. 1).

Table 1 summarizes the payload mass and inertia characteristics, the payload initial angular rates, and the coordinates of the tether attachment point. Figure 1 also gives a schematic representation of the payload accommodation on board the Delta second stage and of the payload flight configuration. It is worth noting that the body axes have been taken so that they tend to align with the axes of the orbiting reference frame when the payload reaches its flight configuration. This means that the payload yaw and roll angles have initial values of −90 and 90 deg, respectively.

Numerical Model

In the numerical model, the tether is simulated by means of lumped masses placed at equidistant positions. Each lump is acted upon by external forces and the tether tension. The area and mass of each lump are those of the tether segment connecting it to the upper adjacent lumped mass. The payload and Delta second stage are simulated with two lumped masses as well. The tether elasticity and structural damping are simulated by means of massless springs and dashpots connecting the lumped masses.[8]

The system orbital motion is described by the force-balance differential equations, the unknown quantities being the components of the position and velocity vectors in a right-handed orbiting reference frame (in which the origin coincides with the initial position of the system center of mass, the z_0 axis is along the local vertical and directed downward, the y_0 axis is perpendicular to the orbital plane, and the x_0 axis is directed forward). This frame rotates with constant orbital rate and radius with respect to the right-handed inertial reference frame (in which the origin is the Earth's center, the X axis points toward the vernal equinox, the Z axis points toward the north pole, and the Y axis completes the right-handed reference frame).

The payload attitude dynamics is computed by integrating the kinematic equations and the Euler equations. The kinematic equations express the time evolution of the payload Euler angles with respect to the inertial reference frame. The Euler equations relate the time derivative of the payload angular rates to the external torques. The torques considered are the tether viscoelastic force, the gravity gradient, the aerodynamic drag, and the attitude control.

Atmosphere Model

Atmosphere parameters, such as density, temperature, and composition, vary with the solar cycle, solar and geomagnetic activity, day, and season.[3] To analyze the influence of the atmosphere on the system dynamics, the Mass-Spectrometer Incoherent-Scatter-1986 (MSIS-86) neutral atmosphere model[9] has been implemented in the numerical code. This model provides the neutral temperature, the densities of the various atmospheric constituents (atomic oxygen included), and the seasonal and local time variations of the geomagnetic activity.

Aerodynamic Drag Model

The aerodynamic force on the ith lumped mass has been computed according to the following expression[10]:

$$\boldsymbol{D}_i = -\tfrac{1}{2}\rho c_D V_i^2 A_i (\hat{\boldsymbol{N}}_i \cdot \hat{\boldsymbol{V}}_i)\hat{\boldsymbol{V}}_i \tag{1}$$

For altitudes greater than 140 km, free-molecular flow prevails. In this case, a value of 2.2 can be assumed for the drag coefficient of satellites of compact shapes. This value also allows for the fact that the satellite may be tumbling.[11]

Atmospheric Density Measurement

Data on SEDS deployment dynamics are collected by means of the payload onboard instrumentation. Table 2 shows the characteristics of the instruments onboard the SEDS-1 end mass.[12] In particular, the three-axis accelerometer can be used to measure the payload nongravitational accelerations. In future tethered atmospheric missions,[13] the accelerometer data can be completed and validated by the data provided by a neutral-mass spectrometer.

In the following, the acceleration levels on board the payload are numerically evaluated by separating the contributions of the aerodynamic drag and the tether tension. Then, the possibility to perform atmospheric density measurements with the end-mass accelerometers is investigated.

Density Measurement from Drag Acceleration

Accelerometer data offer the possibility of achieving measurements of the atmospheric mean density and of the density fluctuations. In particular, the knowledge of the atmospheric density fluctuations is of great importance in view of the strong constraint on the satellite design imposed by the drag levels at low altitudes.[14,15]

Assuming the three-axis accelerometer is at the payload center of mass, the nongravitational acceleration vector measured onboard the payload can be expressed as follows:

$$\boldsymbol{a}_{\text{c.m.}} = \boldsymbol{a}_D + \boldsymbol{a}_T = (\boldsymbol{D}_p/m_p) + (\boldsymbol{T}/m_p) \tag{2}$$

The first term on the right-hand side of Eq. (2) represents the contribution of the aerodynamic drag acting on the payload. The second term, which depends on the tether tension at the payload, simulates the effects of the tether on the payload acceleration levels. Since the body components of the tether tension are measured by the three-axis load cell onboard the payload, it is possible to evaluate the contribution of the aerodynamic drag in Eq. (2). The measurement of the atmospheric density from drag acceleration can then be obtained:

$$a_D = \left(\frac{1}{2}\frac{A_p}{m_p}V^2_{\text{c.m.}}\right)\rho c_D \tag{3}$$

From the measurement of a_D it is possible to compute the product ρc_D, where the drag coefficient can be evaluated on the basis of analytical and experimental results.[11]

Table 2 SEDS-1 end-mass instrumentation

	Range	Resolution
Accelerometer		
Low scale	±1 mg	8.3 μg
Medium scale	±5 mg	42 μg
High scale	±50 mg	0.42 μg
Load cells		
Low scale	±0.1 N	0.83 mN
Medium scale	±1 N	8.3 mN
High scale	±10 N	83 mN
Magnetometer	±600 mG	±4.7 mG

Table 3 Launch date and time, and orbital parameters at the deployment

Launch date	March 23, 1993
Launch time, GMT	04:12
Semimajor axis, km	6835.145
Orbit eccentricity	0.04
Orbit inclination, deg	33.96
Longitude of the asc node,[a] deg	218.5
Argument of perigee, deg	182
Time since perigee passage, s	2661.28

[a]Evaluated with respect to the launch meridian.

Acceleration-Level Analysis

To simulate the tether dynamics accurately, 11 masses have been lumped at equidistant positions along the tether. The values of the orbital parameters at the beginning of the deployment and the launch date and time are listed in Table 3.

Figure 2 shows the first component in the body reference frame (1 axis) of the acceleration measured at the payload center of mass, due to the atmospheric drag. At the orbit perigee, the acceleration due to the aerodynamic drag increases and becomes of the same order of magnitude as the acceleration due to the tether tension. Figure 3 shows a comparison between the moduli of the accelerations due to the aerodynamic drag and the tether tension around the orbit perigee. Figure 4 shows the mean atmospheric density, as well 10% of the density, compared with the finest resolution of the three-axis accelerometer (Table 2). One can see that measurements of the atmospheric mean density from drag acceleration can be obtained only in a time interval of about 700 s around the perigee passage.

With regard to the atmospheric density fluctuations, and considering the short duration of SEDS-1 flight, statistical studies[14] show that only density fluctuations of 5–10% of the full amplitude could be observed near the orbit perigee. On the other hand, Fig. 4 shows that the acceleration levels related to these density fluctuations are lower than the finest resolution of the onboard accelerometers. Density fluctuations can, then, be detected only by reducing the perigee altitude, by increasing the number of perigee passages, and by improving the resolution of the payload onboard accelerometers. In addition, since the density fluctuations vary with the altitude, latitude, and geomagnetic and solar activity, atmospheric data have to be collected at many different combinations of orbit inclinations, altitudes, solar times, geomagnetic conditions, and geographic locations, by using the opportunity of frequent flight offered by Delta launch vehicles.

End-Mass Attitude Dynamics

The analysis performed in Ref. 16 shows that the payload attitude dynamics is characterized by large amplitudes both in the initial

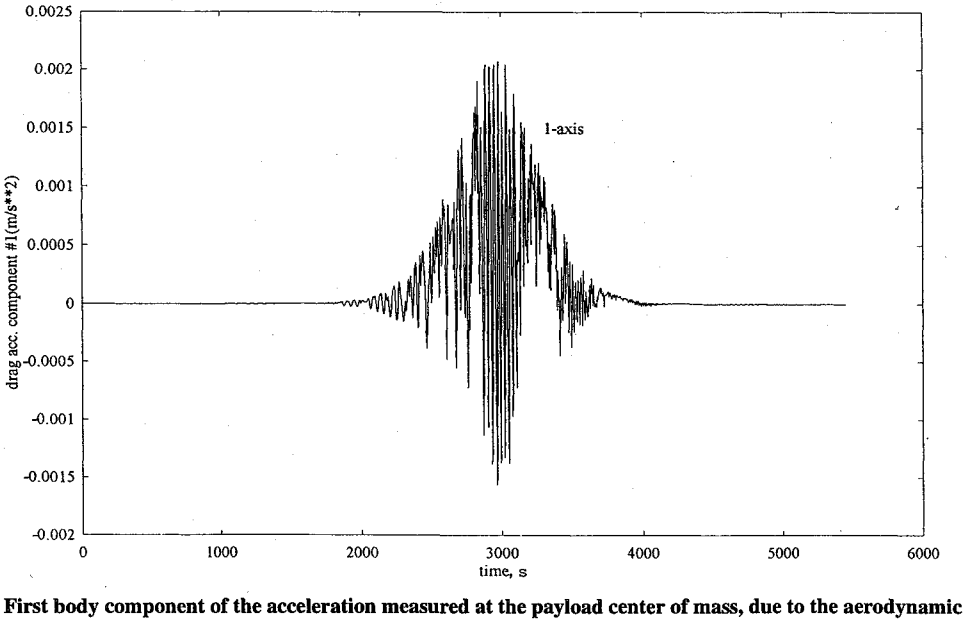

Fig. 2 First body component of the acceleration measured at the payload center of mass, due to the aerodynamic drag.

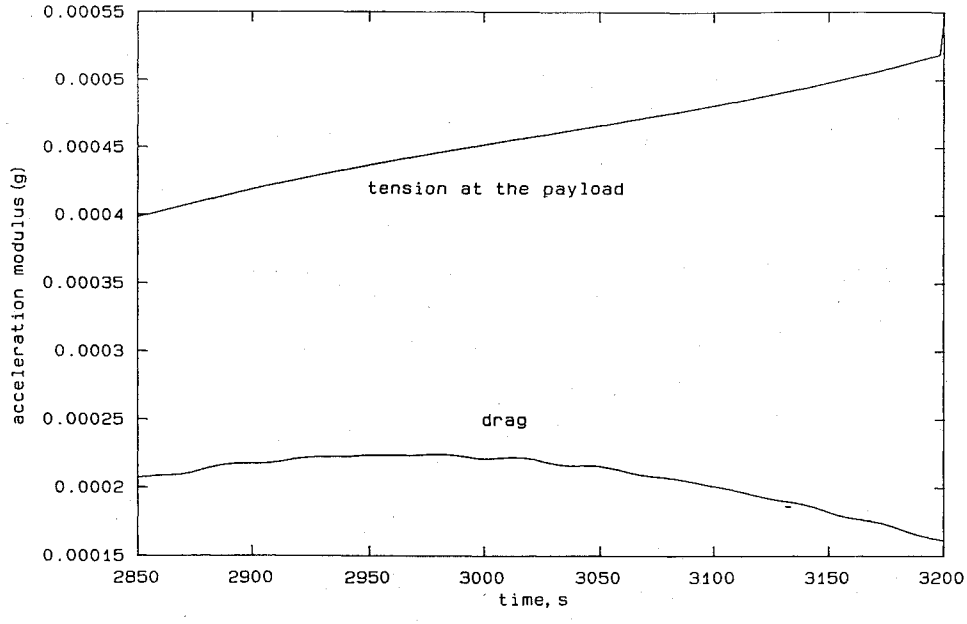

Fig. 3 Moduli of the accelerations due to the tether tension and the aerodynamic drag in a time interval around the orbit perigee.

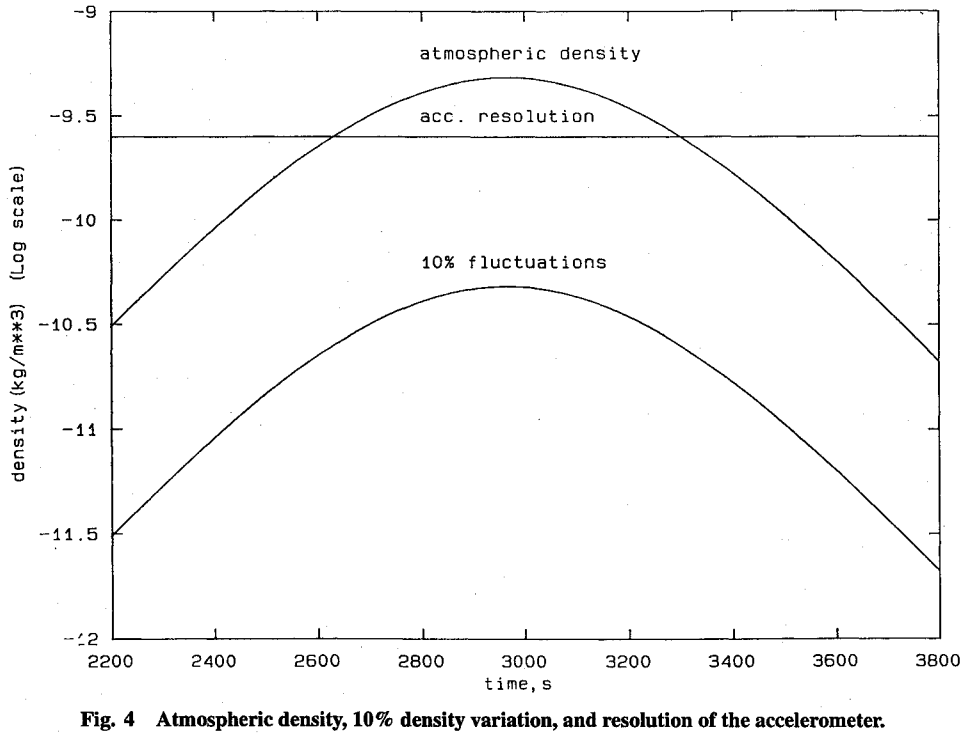

Fig. 4 Atmospheric density, 10% density variation, and resolution of the accelerometer.

phase and, despite of the increasing tension, in the final phase of the deployment. This behavior is caused by the payload initial conditions at ejection as well as the lack of adequate restoring torques.[17] These factors severely limit the use of the SEDS payload as a scientific platform if no attitude control is provided.

Preliminary Analysis of Attitude Control

Several investigators have analyzed the operating requirements and instrument complement for an upper-atmospheric observation payload.[18] The use of tethered observing platforms places unconventional requirements on system design factors such as attitude knowledge and control and dynamic isolation.

As shown in Refs. 19 and 20, the measurement of the accommodation and drag coefficients with an accuracy of 10–20% requires attitude control within ±2 deg. However, attitude control within ±10–20 deg should be provided to perform a postprocessing correction of the data by removing the effects of the short-term and long-term dynamics. Considering the short duration of SEDS-1 missions at low altitudes, the attitude high frequencies due to the tether tension torque, in particular, need to be controlled. An analysis of attitude stabilization and control techniques is performed by making use of both analytical models and numerical simulations.

Attitude Control at Payload Ejection

The numerical simulations showed that the main causes of the observed large attitude amplitudes are the initial conditions at the deployment and the low-tension deployment strategy. A system of thrusters can be used to damp the rotational kinetic energy gained by the payload in the short initial phase of the deployment, in which it approaches its flight configuration.

A preliminary estimate of the moduli of the attitude-control torques has been made by considering the initial conditions of the deployment. By considering only the torque due to the tether tension,

Table 4 Attitude-control torques and required thrusts in the case of control with thrusters

Body axis	Max. attitude excursion, deg	Max control torque, Nm	Required thrust, N
1	±1	7.16×10^{-2}	4.42×10^{-1}
2	±1	1.92×10^{-3}	1.03×10^{-2}
3	±1	1.74×10^{-1}	9.31×10^{-1}

Table 5 Payload initial angular rates and tether attachment-point coordinates in the case of attitude control

Initial angular rates, deg/s		Attach-point coordinates, m	
Symbol	Value	Symbol	Value
ω_1	−0.592	x_1	0
ω_2	−0.513	x_2	0
ω_3	0	x_3	−0.094

the following expressions can be obtained for the maximum values of the body components of the attitude-control torques[10]:

$$M_{c1\,\max} = \frac{1}{2}\frac{\omega_1^2 I_1}{\alpha_{\max}} + x_3 T\cos\delta + x_2 T\sin\delta \tag{4a}$$

$$M_{c2\,\max} = \frac{1}{2}\frac{\omega_2^2 I_2}{\beta_{\max}} - x_1 T\sin\delta \tag{4b}$$

$$M_{c3\,\max} = \frac{1}{2}\frac{\omega_3^2 I_3}{\gamma_{\max}} - x_1 T\cos\delta \tag{4c}$$

Table 4 summarizes the numerical values of the attitude-control torques and of the required thrusts, obtained assuming the payload ejection angle constant and equal to 10 deg. Since the use of thrusters is limited to a short initial phase of the deployment, only low thrusts and low fuel consumption are required to damp the initial rotational kinetic energy of the payload.

Attitude Passive and Active Control

In the following paragraphs, techniques for passive and active control of SEDS's end-mass attitude dynamics are analyzed. In particular, the use of a rigid boom, of two symmetric fins for drag stabilization, and of the mobile tether attachment point is described.

Attitude Analytical Model

The end-mass attitude control has been analyzed by placing the tether attachment point in a symmetrical position with respect to the payload center of mass, as in Fig. 5. This figure also gives a schematic representation of the payload with a rigid boom and two fins symmetrically positioned along the 2 axis of the body reference frame for drag stabilization.

The numerical simulations show that a change in payload geometry and initial attitude rates smaller than the nominal case (e.g., by turning the thrusters on at the beginning of the deployment) result in a more stable attitude dynamics. Table 5 gives the new coordinates of the tether attachment point and the initial values of the payload angular rates considered in the numerical simulation of the attitude control. As shown in Fig. 5, the payload principal axes are initially aligned with the axes of the orbiting reference frame.

Although the numerical simulation showed that large amplitudes characterize SEDS's end-mass attitude history, with reference to the new configuration in Fig. 5, a preliminary estimate of the required attitude control torques can be obtained by assuming that the angles are small. However, as will be shown in the numerical analysis, this assumption can be considered valid for the high-frequency attitude rotations due to the tether tension torque, of particular interest in our case. Therefore, the payload attitude equations become[21]

$$\ddot{\alpha} + \left(4\Omega^2 k_1\right)\alpha - (1-k_1)\Omega\dot{\gamma} = M_1/I_1 \tag{5a}$$

$$\ddot{\beta} + \left(3\Omega^2 k_2\right)\beta = M_2/I_2 \tag{5b}$$

$$\ddot{\gamma} + \left(\Omega^2 k_3\right)\gamma + (1-k_3)\dot{\alpha} = M_3/I_3 \tag{5c}$$

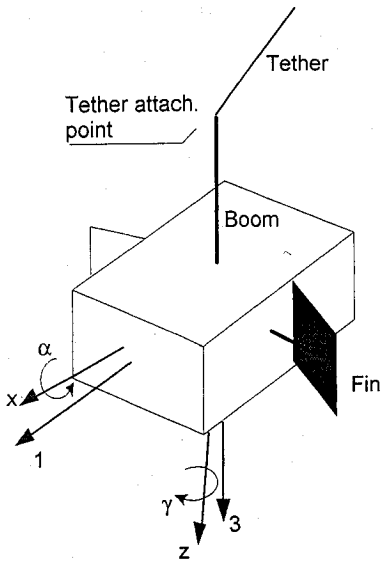

Fig. 5 Schematic representation of the payload with rigid boom and fins for drag stabilization.

where the inertia ratios k_i and the external torques M_i are given by

$$k_1 = (I_2 - I_3)/I_1 \tag{6a}$$

$$k_2 = (I_3 - I_1)/I_2 \tag{6b}$$

$$k_3 = (I_1 - I_2)/I_3 \tag{6c}$$

and

$$M_1 = -x_3 T_1\alpha - (x_3 T_1/l_1)\varepsilon_2 + M_{e1} \tag{7a}$$

$$M_2 = -x_3 T_1\beta - (x_3 T_1/l_1)\varepsilon_1 + M_{e2} \tag{7b}$$

$$M_3 = M_{e3} \tag{7c}$$

In Eqs. (7), the tether restoring torques and the disturbing torques due to the tether lateral deflections and the external perturbations have been considered.

Attitude Stabilization with a Rigid Boom

The payload attitude dynamics can be passively stabilized by means of a rigid boom at the tether attachment point (Fig. 5).[17] By introducing the boom length B into Eqs. (5) and (7) and by applying the final-value theorem to the pitch equation, the following expression can be obtained for B:

$$B = -x_3\left(1 - \frac{\varepsilon_{1\,\max}}{l_1\beta_{ss}}\right) - 3\Omega^2 k_2\frac{I_2}{T_1} + \frac{M_{e2\,\max}}{T_1\beta_{ss}} \tag{8}$$

Note that a similar expression for B can be obtained from the roll equation. Figure 6 shows the values of B in meters vs the pitch-angle final value for $l_1 = 2500$ m and $\varepsilon_{1\,\max} = 200$ m. Note that only the control of the attitude high frequencies caused by the tether-tension torque has been considered (i.e., $M_{e2\,\max} = 0$). From Fig. 6 it is possible to obtain a preliminary estimate of the boom length necessary for the required attitude control.

Drag Stabilization

The numerical simulations have shown that at the orbit perigee the aerodynamic forces on the payload are large enough for passive attitude stabilization by the aerodynamic drag.[22] A typical arrangement producing yaw-axis aerodynamic stabilization is shown in Fig. 5, where two fins have been symmetrically positioned with respect to the payload center of mass. In the analysis, the use of a tail at the back of the payload, as in the case of the TSS-2 subsatellite, is not considered, on account of the reduced space available for the payload on the Delta second stage.[23]

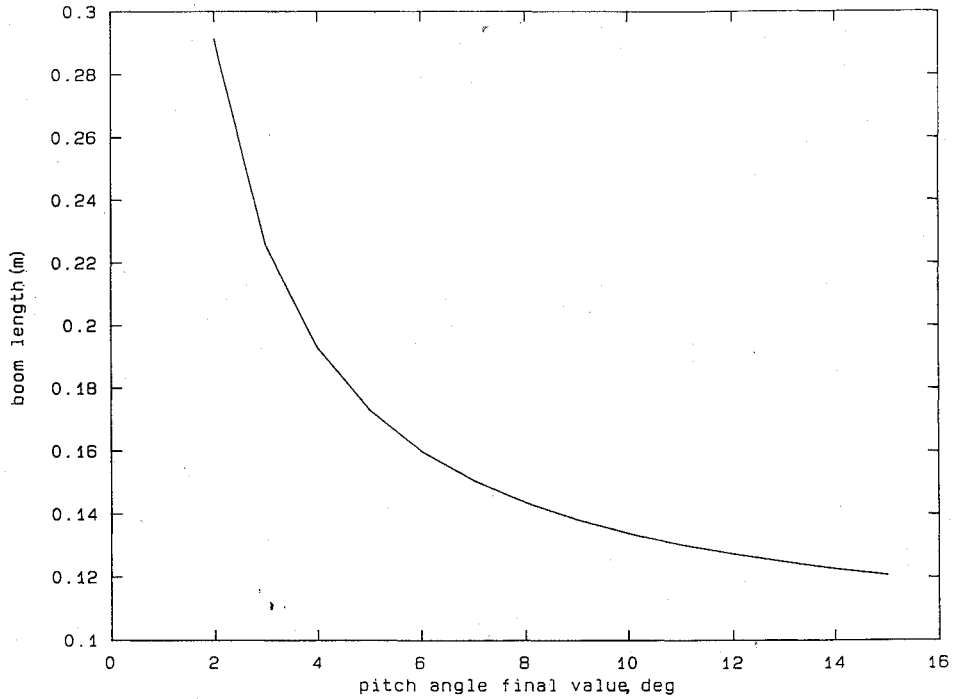

Fig. 6 Boom length vs pitch-angle final value.

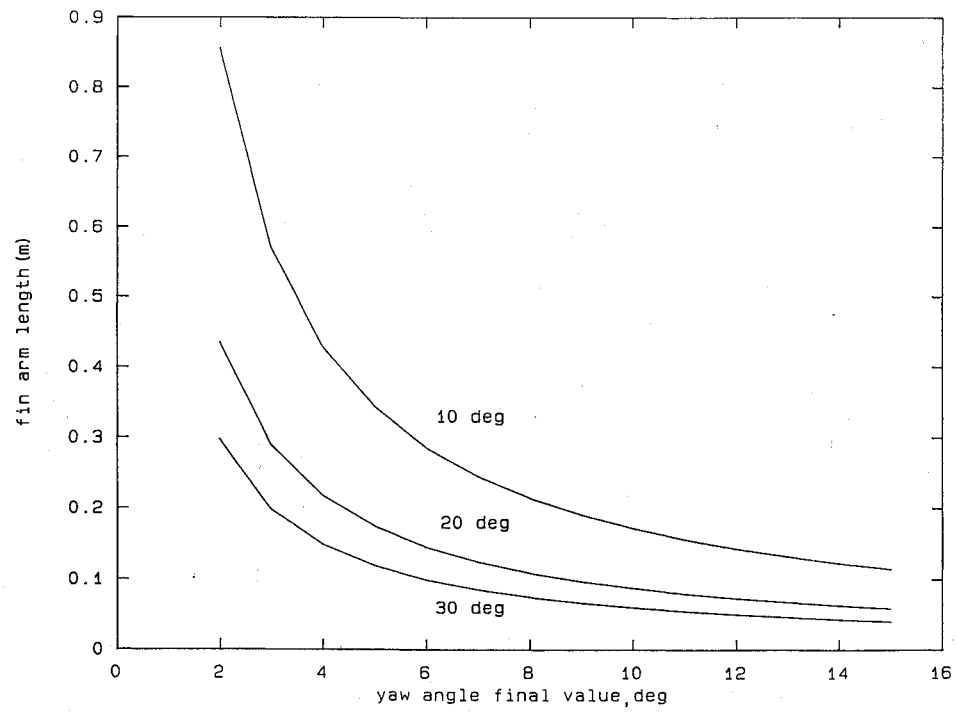

Fig. 7 Fin arm length vs yaw-angle final value.

By evaluating the body components of the aerodynamic torque due to the fins, and by applying the Laplace transformation to the roll and yaw equations (5a) and (5c), we have in matrix form

$$\begin{bmatrix} \dfrac{M_1(s)}{I_1} \\ \dfrac{M_2(s)}{I_2} \end{bmatrix} = \begin{bmatrix} s^2 + \left[4k_1\Omega^2 + (T_1x_3/I_1)\right] & -\Omega(1-k_1)s \\ \Omega(1-k_3)s & s^2 + \left(\Omega^2k_3 + H\right) \end{bmatrix} \begin{bmatrix} \alpha(s) \\ \gamma(s) \end{bmatrix} \tag{9}$$

where

$$H = \frac{\rho c_D V_{\text{c.m.}}^2 A_F d}{I_3} \sin\eta \tag{10}$$

By applying the final-value theorem to Eq. (9), the following expressions can be obtained for the steady-state values of the roll and yaw angles:

$$\alpha_{ss} = \frac{M_{1\max}}{I_1\left[4\Omega^2k_1 - (Tx_3/I_1)\right]} \tag{11a}$$

$$\gamma_{ss} = \frac{M_{3\max}}{I_3\left(\Omega^2k_3 + H\right)} \tag{11b}$$

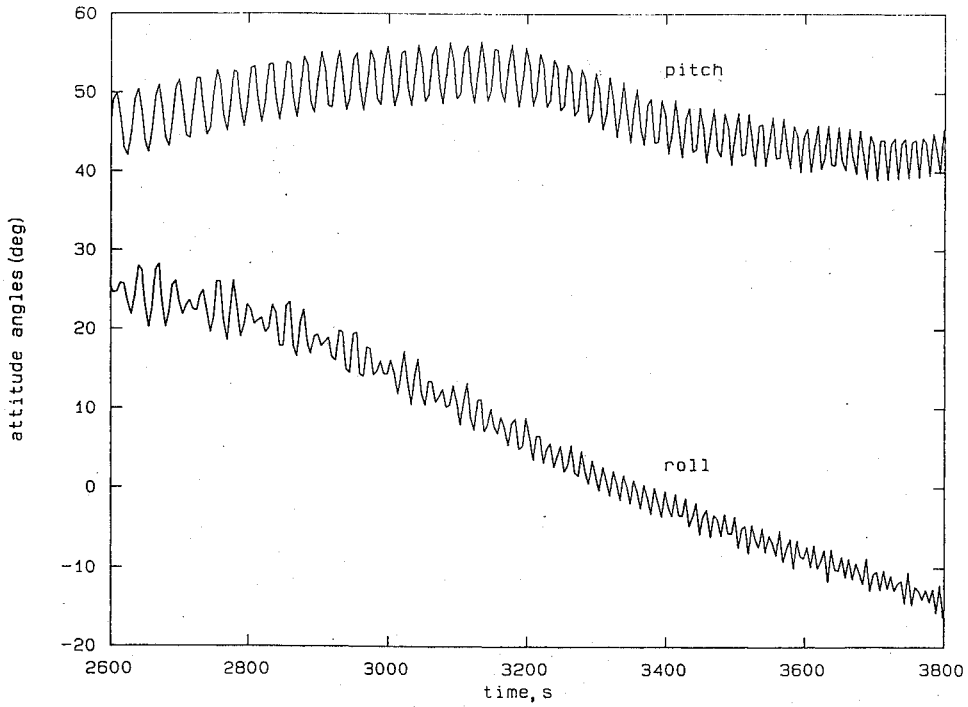

Fig. 8 Payload pitch and roll angles after control with a 20-cm-long rigid boom.

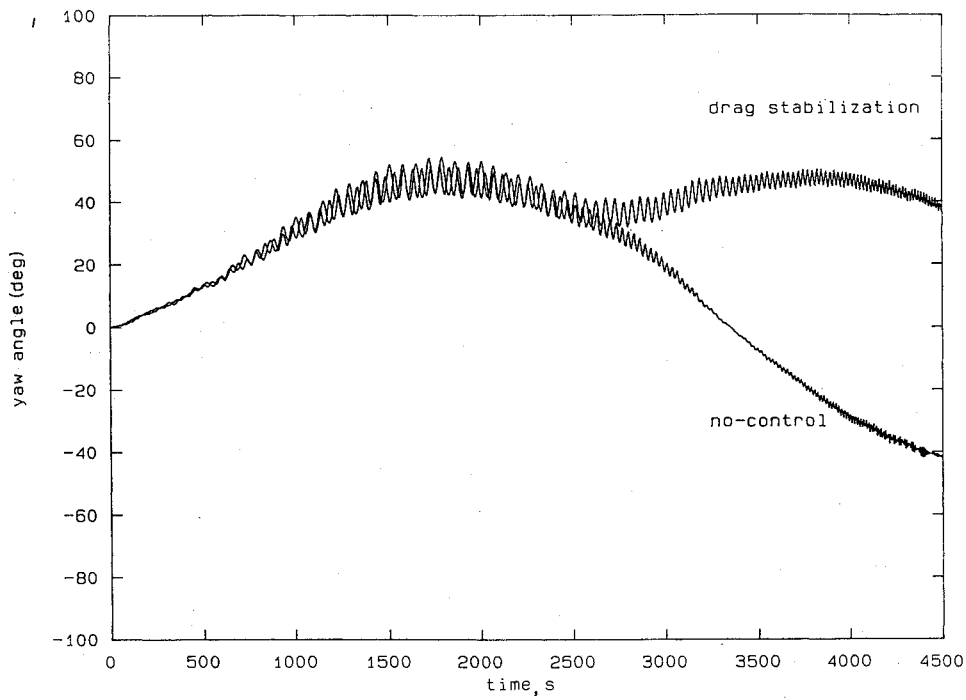

Fig. 9 Payload yaw angle without and with the use of fins for drag stabilization.

The length of the fin arm can then be obtained from Eq. (11a) as

$$d = \frac{1}{\rho c_D V_{\text{c.m.}}^2 A_F}\left[\frac{M_{3\max}}{\gamma_{ss}} - \Omega^2 k_3 I_3\right]\frac{1}{\sin\eta} \tag{12}$$

From Fig. 7 it is possible to obtain a preliminary estimate of d in meters as a function of the yaw-angle steady-state value for different values of η and $A_F = A/2$. These quantities have been computed by adopting a value of 4.8×10^{-12}kg/m^3 for the atmospheric density.

Control with the Mobile Attachment Point

When stringent attitude control is required, an active control technique based on the displacement of the tether attachment point on the payload can be used to damp the attitude high frequencies. Of course, in this case, onboard attitude sensors and feedback control logic are required.[21]

By introducing the torques due to the displacement of the tether attachment point, Eqs. (7) become

$$M_1 = -x_3 T_1 \alpha - (x_3 T_1 / l_1)\varepsilon_2 + x_2 T_1 + M_{e1} \tag{13a}$$

$$M_2 = -x_3 T_1 \beta - (x_3 T_1 / l_1)\varepsilon_1 + x_1 T_1 + M_{e2} \tag{13b}$$

$$M_3 = -x_1 T_1 \alpha - x_2 T_1 \beta + M_{e3} \tag{13c}$$

As in Ref. 21, the attitude control can be performed by moving

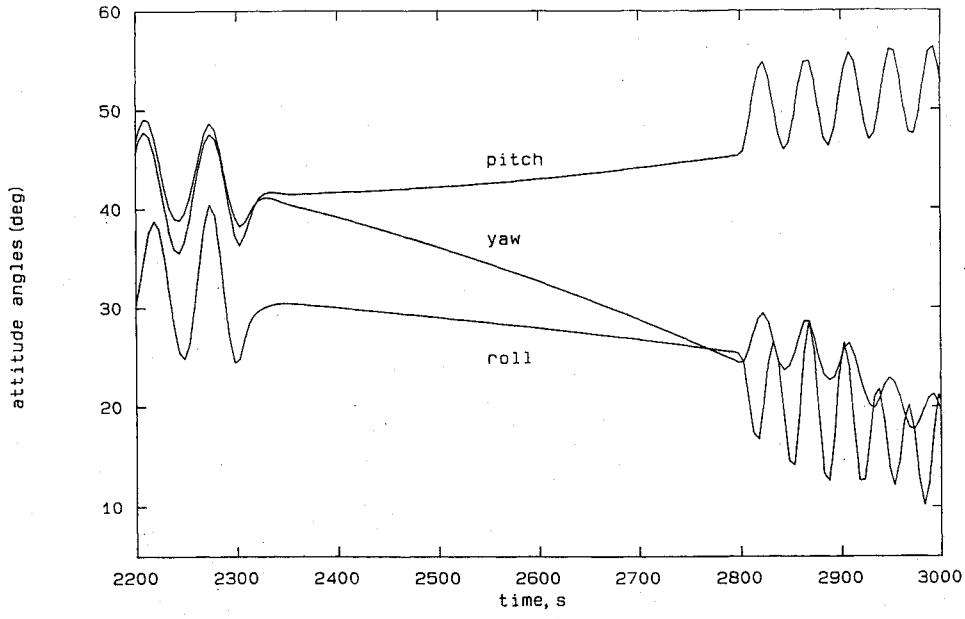

Fig. 10 Payload attitude control with the mobile attachment point in a time interval around the orbit perigee.

the tether attachment point according to the following control laws:

$$x_1 = k_\beta \beta + k_\beta \tau_\beta \dot{\beta} \tag{14a}$$

$$x_2 = k_\alpha \alpha + k_\alpha \tau_\alpha \dot{\alpha} \tag{14b}$$

where the pitch and roll angles and the respective derivatives have been used as feedback variables. As in Ref. 21, the control-law gains and time constants have been computed assuming a unit damping factor and ±1 deg as the steady-state error for the pitch and roll angles.

Numerical Analysis

Numerical simulations of SEDS-1 end-mass attitude control have been run by using the results of the analytical models. The values adopted for the payload initial angular rates and for the coordinates of the tether attachment point are listed in Table 5.

Figure 8 shows the payload pitch and roll angles in a time interval around the orbit perigee after a 20-cm-long rigid boom has been added to the tether attachment point. It is possible to observe a significant reduction in the amplitudes of the attitude high frequencies, which, because of the increasing tether tension, become approximately 5 deg at the end of the deployment. Because of the deployment strategy, the pitch angle oscillates with low amplitude around a mean value of about 45 deg. Finally, because of the coupling with the roll dynamics, a significant reduction has been observed also in the amplitudes of the high frequencies of the yaw angle, which is not plotted in Fig. 8.

Figure 9 shows the yaw angle of the end-mass in the two cases of noncontrolled attitude dynamics and drag stabilization by means of two symmetrical fins positioned at a distance of 16 cm from the payload center of mass. A value of 10 deg has been assumed for the fin angle η. In the controlled case, as soon as the payload reaches the orbit perigee, the drag stabilization acts on the yaw dynamics. In fact, the yaw angle oscillates with limited amplitude (about ±10 deg) around a mean value of about 40 deg. Of course, the drag stabilization cannot abate the yaw-angle high frequencies.

Figure 10 shows the results of the application of the control law based on the displacement of the tether attachment point on the payload, in a time interval around the orbit perigee. It is possible to see that, in this case, the attitude high frequencies are completely damped. In addition, the roll-angle control has a positive effect also on the damping of the yaw-dynamics high frequencies.

Conclusions

The utilization of SEDS deployed payloads as scientific platforms for atmospheric research has been analyzed. The possibility of performing measurements of the atmospheric density with the accelerometers onboard SEDS payload has been investigated. Results of numerical simulations of SEDS first mission show that measurements of the atmospheric mean density can be obtained only over a short time interval (about 700 s) around the orbit perigee. Measurements of the atmospheric density fluctuations can be achieved only by reducing the altitude of the orbit perigee and/or by using more sensitive accelerometers onboard the payload.

The payload attitude dynamics and control have been investigated. A preliminary analysis of passive and active control devices has been performed analytically and numerically. The results show that the use of passive-control devices, such as rigid booms and fins for drag stabilization, limits the amplitudes of the attitude angles within about ±5–10 deg. Nevertheless, the effectiveness of rigid booms is limited by the lengths required to perform finer attitude control, and the use of fins for drag stabilization is complicated by the small dimensions of the payload and by the small space available for end-mass accommodation on the Delta second stage. Therefore, future atmospheric and/or remote sensing applications, which have very stringent attitude-control requirements, can be only performed by using active-control devices. To this end, a technique based on the displacement of the tether attachment point at the payload seems to be effective. In this case, the attitude high frequencies are completely abated.

Acknowledgments

Mario Cosmo's support has been provided by NASA Marshall Space Flight Center Contract NAS8-36606. Michele Grassi's work has been supported by the Agenzia Spaziale Italiana and the Italian Ministry for University and Research.

References

[1]Anderson, J. L., "Outer Atmospheric Research Using Tethered Systems," *Journal of Spacecraft and Rockets*, Vol. 26, No. 2, 1988, pp. 66–71.

[2]Hurlbut, F. C., and Potter, J. L., "Tethered Aerothermodynamic Research Needs," *Journal of Spacecraft and Rockets*, Vol. 28, No. 1, 1991, pp. 50–57.

[3]Brown, K. G., Melfi, L. T., Jr., Upchurch, B. T., and Wood, G. M., "Downward-Deployed Tethered Satellite Systems, Measurements Techniques, and Instrumentation: A Review," *Journal of Spacecraft and Rockets*, Vol. 29, No. 5, 1992, pp. 671–677.

[4]Carroll, J. A., "The Small Expendable Deployment System (SEDS)," *Space Tethers for Science in the Space Station Era*, edited by L. Guerriero and I. Bekey, Vol. 14, Societá Italiana di Fisica, 1987, pp. 43–50.

[5]Harrison, K. J., Rupp, C. C., Carroll, J. A., Alexander, C. M., and Pulliam, E. R., "Small Expendable-Tether Deployment System (SEDS) Development Status," *Tethers in Space Toward Flight, Proceedings of the Third International Conference on Tethers in Space* (San Francisco, CA), AIAA, Washington, DC, 1989, pp. 19–26 (AIAA Paper 89-1550).

[6]Lorenzini, E. C., and Carroll, J. A., "In-Orbit Experimentation with the Small Expendable-Tether Deployment System," *ESA Journal*, Vol. 15, 1991, pp. 27–33.

[7]Wood, G. M., Siemers, P. M., Squires, R. K., and Wolf, H., "Downward-Deployed Tethered Platforms for High-Entalpy Aerothermodynamic Research," *Journal of Spacecraft and Rockets*, Vol. 27, No. 2, 1990, pp. 216–221.

[8]Vetrella, S., Moccia, A., Lorenzini, E. C., and Cosmo, M. L., "Attitude Dynamics of the Tether Elevator/Crawler System for Microgravity Applications," *ESA Journal*, Vol. 14, No. 3, 1990, pp. 303–312.

[9]Hedin, A. E., "MSIS-86 Thermospheric Model," *Journal of Geophysical Research*, Vol. 92, No. A5, 1987, pp. 4649–4662.

[10]Wertz, J. R. (ed.), *Spacecraft Attitude Determination and Control*, D. Reidel, Dordrecht, The Netherlands, 1980, pp. 573, 574.

[11]Moe, M. R., Wallace, S. D., and Moe, K., "Refinements in Determining Satellite Drag Coefficients: Method for Resolving Density Discrepancies," *Journal of Guidance, Control, and Dynamics*, Vol. 16, No. 3, 1993, pp. 441–445.

[12]DeLoach, R., Diamond, J., Finley, T., and Rhew, R., "End-Mass Instrumentation for First SEDS/Delta-II Mission," AIAA Paper 90-0537, Jan. 1990.

[13]Blanchard, R. C., Hendrix, M. K., Fox, J. C., Thomas, D. J., and Nicholson, J. Y., "Orbital Acceleration Research Experiment," *Journal of Spacecraft and Rockets*, Vol. 14, No. 6, 1987, pp. 504–511.

[14]Touboul, P., Bernard, A., Barlier, F., and Berger, C., "Air Drag Effect on Gradiometer Measurements," *Manuscripta Geodaetica*, Vol. 16, Jan. 1991, pp. 73–91.

[15]Hedin, A. E., and Mayr, H. G., "Characteristics of Wavelike Fluctuations in Dynamics Explorer Neutral Composition Data," *Journal of Geophysical Research*, Vol. 92, No. A10, 1987, pp. 11,159–11,172.

[16]Lorenzini, E. C., Gullahorn, G. E., Cosmo, M. L., Grossi, M. D., and Grassi, M., "Analytical Investigation of the Dynamics of Tethered Constellations in Earth Orbit (Phase II)," Smithsonian Institution Astrophysical Observatory, Quarterly Rept. 28, Contract NAS8-36606, Cambridge, MA, June 1992.

[17]Lorenzini, E. C., Gullahorn, G. E., Cosmo, M. L., Bortolami, S. B., Grossi, M. D., and Grassi, M., "Analytical Investigation of the Dynamics of Tethered Constellations in Earth Orbit (Phase II)," Smithsonian Institution Astrophysical Observatory, Quarterly Rept. 32, Contract NAS8-36606, Cambridge, MA, Nov. 1993.

[18]Office of Aeronautics, Exploration and Technology (Ed.), "Aerothermodynamic Research Priorities for Tethered Satellites," Rept. of the TSS-2 Research Priorities Workshop, Feb. 1989, pp. 1–11.

[19]Webster, W. J., "Engineering Tethered Payloads for Magnetic and Plasma Observation in Low Orbit," *Journal of Spacecraft and Rockets*, Vol. 26, No. 2, 1989, pp. 80–84.

[20]Webster, W. J., "Scientific Purposes of Earth Orbital Tether Operations," *Advances in Astronautical Sciences*, Vol. 62, Sept. 1988, pp. 51–61.

[21]Moccia, A., Vetrella, S., and Grassi, M., "Attitude Dynamics and Control of a Vertical Interferometric Radar Tethered Altimeter," *Journal of Guidance, Control, and Dynamics*, Vol. 16, No. 2, 1993, pp. 264–269.

[22]Boettcher, R.-D., Koppenwaller, G., and Legge, H., "Aerodynamic Aspects of Tethered Satellite Design and Utilization," AIAA Paper 89-1562, 1989, pp. 109–114.

[23]"SEDS-1 Mission Specification—Mission Requirements and Vehicle Description," MDC91H0197A, McDonnell Douglas Space System Co., July 1992.

I. D. Boyd
Associate Editor